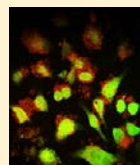# Europium-Doped TiO$_2$ Hollow Nanoshells: Two-Photon Imaging of Cell Binding

Sergio Sandoval,[†,‡,§] Jian Yang,[†,§,‖] Jesus G. Alfaro,[⊥] Alexander Liberman,[†,#] Milan Makale,[§] Casey E. Chiang,[∇] Ivan K. Schuller,[∇] Andrew C. Kummel,*[,‡,§,‖] and William C. Trogler*[,‡,§,‖]

[†]Department of Bioengineering, [‡]CalIT2 Nanomedicine Laboratory, [§]Moores Cancer Center, [‖]Department of Chemistry & Biochemistry, [⊥]Department of NanoEngineering, [#]Program in Materials Science and Engineering, and [∇]Department of Physics, University of California, San Diego, 9500 Gilman Drive, La Jolla, California 92093-0358, United States

ABSTRACT: A simple scalable method to fabricate luminescent monodisperse 200 nm europium-doped hollow TiO$_2$ nanoshell (NS) particles is reported. Fluorophore reporter, Eu^{3+} ions are incorporated directly in the NS matrix, leaving the surface free for functionalization and the core free for payload encapsulation. Amine-functionalized polystyrene beads were used as templates, and the porous walls of europium-doped titania nanoshells were synthesized using titanium(IV) *t*-butoxide and europium(III) nitrate as reactants. X-ray diffraction analysis identified anatase as the predominant titania phase of the rigid nanoshell wall structure, and photoluminescence spectra showed that the Eu(III)-doped TiO$_2$ nanoshells exhibited a red emission at 617 nm due to an atomic f−f transition. Nanoshell interactions with HeLa cervical cancer cells in vitro were visualized using two-photon microscopy of the Eu(III) emission and studied using a luminescence ratio analysis to assess nanoshell adhesion and endocytosis.

200 nm Eu(III) doped TiO$_2$ nanoshells coated with polyethyleneimine adhering to HeLa cervical cancer cells as imaged by two-photon microscopy

KEYWORDS: *two photon, microscopy, titania, nanoshells, europium(III), luminescence, anatase, HeLa, polyethyleneimine, SEM, TEM, DLS*

■ INTRODUCTION

Titania nanomaterials and hybrid derivatives have attracted interest because of their broad range of industrial applications, such as in photovoltaic devices,[1,2] chemical/gas sensors,[3] catalysis,[4,5] wastewater treatment,[6,7] and filtration and sorption media.[8] Titania nanomaterials and their compound hybrid composites are also intriguing for medical applications,[9−15] and several studies of applications in anticancer research[16−19] have appeared. When TiO$_2$ nanoparticles undergo photoexcition with ultraviolet (UV) light, photoinduced electrons and holes are produced. These electrons and holes can react with hydroxyl ions or water to produce reactive hydroxyl radicals ●OH and perhydroxyl radicals HO$_2$●. These oxygen species are also highly reactive with cells and can cause DNA strand breaking with genotoxicity.[16,20] This characteristic gives titania nanomaterials the potential to be used as photodynamic therapy agents in cancer treatments.[21,22] Furthermore, the use of various titania and hybrid titania nanocomposites made up of gold,[23] silver,[24] copper,[25] platinum,[17,26] and iron cooperatives,[12] as well as titania nanoparticles combined with specific antibodies,[27] have been shown to have cancer therapeutic potential typically via photodynamic therapy or magnetic therapy (Fe composites).

Several methods have been described for the synthesis of TiO$_2$ nanospheres. Caruso and co-workers[28,29] used a layer-by-layer (L-b-L) self-assembly technique to fabricate both SiO$_2$ and TiO$_2$ hollow spheres. For the TiO$_2$ spheres, a positively charged TiO$_2$ colloid was used to form a shell around polymer templates through the absorption of polyelectrolytes. Repeated absorption of polyelectrolytes and TiO$_2$ precursors increased the thickness and integrity of the shell wall. Xia et al.[30] prepared hollow TiO$_2$ spheres by using crystalline arrays of polystyrene beads as a template. Well-defined TiO$_2$ spheres could be fabricated from these methods, but multiple steps are needed, which makes these methods challenging for the large-scale fabrication needed in biomedical applications. Similar templating methods using activated carbon[31] or polymers[32−35] as cores have also been reported. Alternative methods, such as ultrasonic spray pyrolysis,[36] diffusion flame synthesis,[37] and supercritical fluid methods,[38,39] have been used as potentially scalable routes to create TiO$_2$ spheres. These processes tend to produce nanoparticles with a range of sizes and/or have fragile shell structures.

Another active research area has been the development of nanoparticles that incorporate rare-earth ions within their structures. Rare-earth materials have attractive properties that include increased photostability, reduced light scattering, narrow emission spectra, large emissive Stokes shifts, and long luminescence lifetimes and allow for simple functionalization strategies.[40,41] Europium is particularly advantageous because europium(III) ions produce red photoluminescence with narrow atomic emission profiles when doped into inorganic lattices. Due to its high transparency to visible light and its robust thermal, chemical, and mechanical properties,[42−44] titania is an ideal host material for Eu^{3+}, and several Eu^{3+}-doped TiO$_2$ films, nanocrystals, and particles have been

ACS Publications © 2012 American Chemical Society

4222

dx.doi.org/10.1021/cm302642g | *Chem. Mater.* 2012, 24, 4222−4230

reported.[42,43,45−52] Furthermore, europium provides an inexpensive, long lifetime, low cytotoxicity, and safe method for fluorescence imaging compared to organic fluorophores.[40,53] The high efficiency of reactive oxygen production during near-UV irradiation of TiO_2 leads to enhanced photobleaching of organic dyes[54] in aerobic environments.

This paper describes a simple method of synthesizing uniform monodisperse europium(III)-doped hollow TiO_2 nanoshells (NSs) that have rigid porous shell walls. The utility of this NS design is that the long-lived fluorophore reporter, Eu^{3+} ions are incorporated directly in the NS matrix, leaving the surface free for functionalization and the NS core free for payload encapsulation. Amine-functionalized polystyrene (PS) beads were used as templates in the synthesis. Titanium(IV) *t*-butoxide was used as the precursor for titania deposition to reduce the rate of hydrolysis and suppress nontemplated growth. The sol−gel hydrolysis of titanium(IV) *t*-butoxide was catalyzed on the surface of amine-functionalized PS beads to form a thin porous titania coating. Doping was effected by using ethanol solvent containing 5% water and dissolved europium(III) nitrate. After removing the PS core by calcination, hollow nanoporous TiO_2 NSs with red luminescence characteristic of doping by Eu^{3+} were isolated. This protocol provides a simple, inexpensive, and scalable method to prepare Eu^{3+}-doped titania NSs for imaging studies. These nanoshells were coated with a cationic polymer, poly-(ethylenimine) (PEI), to alter the surface charge from negative to positive, which allowed the NS to adhere to HeLa cervical cancer cells. Cell to NS interactions were imaged using two-photon (2-P) microscopy and quantified using a previously reported luminescence ratio analysis.[55]

■ EXPERIMENTAL METHODS AND MATERIALS

Materials. Titanium(IV) *t*-butoxide, europium(III) nitrate hydrate, and poly(ethylenimine) (PEI - MW 750 000) were obtained from Aldrich-Sigma Ltd. The 200 nm amine-functionalized polystyrene beads (2.5% w/w) were purchased from PolySciences Ltd. HeLa cervical cancer cells were purchased from ATCC (Manassas, Virginia); Dulbecco's Phosphate Buffer Saline solution (DPBS 1 ×), Dulbecco's Modified Eagle's Medium (DMEM), and fetal bovine serum (FBS) were purchased from Mediatech, Inc. (Manassas, Virginia). Media supplements, chloromethylfluorescein diacetate (CMFDA) CellTracker Green intracellular stain, and Prolong Gold were obtained from Invitrogen (Carlsbad, California). Nunc Lab-Tek II 4-well chamber slides and paraformaldehyde (PFA) were purchased from Thermo-Fisher Scientific (Fair Lawn, New Jersey). All chemicals and reagents were used as received or as described in manufacturer protocols, unless otherwise stated.

Preparation of Europium-Doped Hollow Titania Nanoshells. In a 2 mL Eppendorf tube, 0.25 mg of $Eu(NO_3)_3 \cdot 5H_2O$ was dissolved in 1.25 mL of absolute ethanol. A 50 uL portion of a 2.5% weight dispersion (in water) of 200 nm aminopolystyrene beads was added. Next 25 uL of 1 M titanium(IV) *t*-butoxide/ethanol solution was added, and the mixture was stirred in a vortex mixer for 5 min at room temperature at a setting of 900 rpm. The suspended core−shell nanospheres were collected by centrifugation, washed with ethanol, and dried in vacuum for 48 h at room temperature to give 1.90 mg of core−shell spheres.

The aminopolystyrene bead core was removed by calcining the preceding nanospheres by heating in air at 5 °C per minute to 500 °C and maintaining this temperature for 24 h. About 0.85 mg of europium-doped hollow TiO_2 NSs were recovered as a white-pink powder. Energy-dispersive X-ray spectroscopy (EDS) showed the Eu content of this preparation was 0.84% (mol %).

Modification of Eu/TiO₂ Hollow Nanoshells with Poly-(ethylenimine). To increase the cell-adhering efficiency of Eu/TiO₂

nanoshells, the NS surface charge was changed from negative to positive using poly(ethylenimine) (PEI). This was accomplished by suspending 3 mg of Eu/TiO₂ NS in 1.5 mL of 0.1 mg/mL PEI in water. The suspension was stirred for 2 h; nanoshells were collected by centrifugation and washed with water. Subsequently, the PEI-coated NSs were suspended in 1.0 mL of DPBS for use in cell imaging experiments.

Characterization of Eu/TiO₂ Hollow Nanoshells. The scanning electron microscopy (SEM) and EDS measurements were conducted on a FEI/Philips XL30 FEG ESEM microscope with an accelerating voltage of 10 kV. The average diameter of the NSs was determined from the SEM images. Transmission electron microscopy (TEM) images were obtained with the use of a JEOL-2000EX (200 kV) cryo-electron microscope with an accelerating voltage of 200 kV. A Perkin-Elmer LS 45 luminescence spectrometer was used to record luminescence emission and excitation spectra. A Zetasizer Nano ZS (Malvern Instruments) was used to measure the dynamic light scattering (DLS) size distribution, the polydispersity index (PDI), and zeta potential of NSs when suspended in distilled water with gentle sonication and vortexing. X-ray powder-diffraction patterns were obtained using a Bruker Discover D8 X-ray diffractometer with a rotating anode Cu Kα (λ = 0.154 nm) source.

Cell Culture. HeLa cervical cancer cells (5×10^4) in Dulbecco's Modified Eagle's Medium (DMEM) supplemented with 10% FBS, 1% antibiotics (penicillin, streptomycin, glutamine (PSG)), and 1% sodium pyruvate were plated per well on Nunc Lab-Tek II 4-well chamber slides at 37 °C in a humidified atmosphere of 5% CO_2. HeLa cells were allowed to grow to 60−80% well confluence before beginning cell adhesion/endocytosis experiments.

Cell Adhesion/Endocytosis Experiments. HeLa cells were incubated with 500 μg/mL of europium−TiO₂ NSs functionalized with PEI for 24 h in DMEM complete media at 37 °C in a humidified atmosphere of 5% CO_2. Cells were then washed 2 times with DPBS and labeled with 2.5 μM CMFDA CellTracker Green intracellular stain in DPBS for 30 min. Cells were washed 3 times with DPBS to remove any surplus dye, fixed with 4% PFA in DPBS solution, washed 2 times more with DPBS, and covered with Prolong Gold antifade reagent to prepare samples for visualization by two-photon microscopy.

Two-Photon (2-P) Microscopy of HeLa Cell Interactions with Europium-Doped Titania Nanoshells in Vitro. 2-P fluorescence dual color (red/green europium TiO₂ NS/CMFDA) images were obtained with a custom-modified Nikon FN1 intravital microscope fitted with a 60x water immersion objective (Nikon, 1.2 NA). The instrument was driven by a Spectraphysics MaiTai Ti:Sa 3 W, 120 fs pulsed laser tuned to 705 nm. The microscope operated in nondescanned mode. Emitted sample light was separated into red/green channels using a beam splitter and band-pass filters (Chroma ET620/60 and ET510/50). Two side-on PMTS (Hamamatsu) captured the light, and the raster scan data were assembled and saved using Nikon EZ-1 display/analysis software. Full-field images were initially acquired at 60x, with constant gain settings between samples, and regions of interest (ROIs) were magnified 3.56x by spatially compressing the raster scan. To confirm the locations of the NSs, image volumes composed of multiple 1 μm XY slices were acquired serially along the sample *z*-axis. 2-P images were further processed for background level and SNR, using Image J (NIH, Bethesda, MD).

■ RESULTS AND DISCUSSION

Synthesis of Eu³⁺-Doped Hollow Titania Nanoshells. Sol−gel reactions are often used to fabricate amorphous inorganic oxides.[56] While primary alkoxysilanes can be hydrolyzed in water slowly, the hydrolysis of primary alkoxylates of titanium(IV) in water is too rapid to use in templating reactions. Therefore, bulky *t*-butoxy groups were employed to slow the rate of hydrolysis, and a solution of ethanol/5% water was used as the reaction medium to reduce the water concentration. These techniques yielded a hydrated
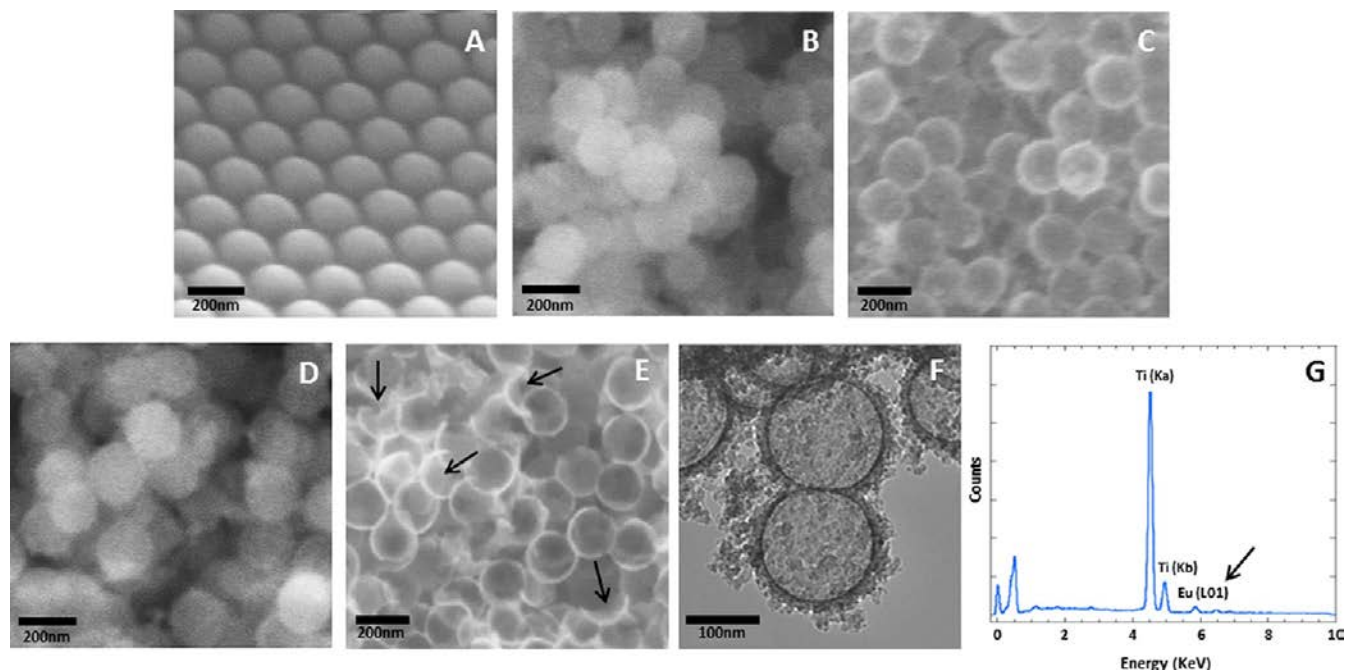
Figure 1. SEM and TEM images of 200 nm plain and europium-doped titania nanoshells prepared using 0.025% Eu(NO$_3$)$_3$·5H$_2$O. A: SEM images of amino polystyrene templates. B: Nondoped TiO$_2$ core−shells. C: Plain TiO$_2$ hollow NSs. D: Eu^{3+}-doped TiO$_2$ core−shells. E: Eu^{3+}-doped TiO$_2$ hollow NS. Small amounts of broken shells in the europium-doped image are identified by black arrows in E. F: TEM image of europium-doped TiO$_2$ hollow NSs showing the some colloidal TiO$_2$ fused on the surface. G: EDS spectrum analysis of Eu^{3+}-doped TiO$_2$ hollow NSs showing X-rays characteristic of both Ti and Eu.

titania sol−gel coating on the amine-functionalized PS beads (Figure 1A and 1B) due to either the negatively charged, partially hydrolyzed sol precursor derived from Ti(O-*t*-Bu)$_4$ being absorbed by the cationic amino groups (partially protonated in water) on the surface of the PS beads or by the unprotonated basic surface amines catalyzing sol−gel hydrolysis. An effort to use plain PS beads to template the TiO$_2$ sol−gel reaction was also attempted, but after the mixture was stirred for 48 h, it was found that no solid shell formed on the nonfunctionalized PS surface.

Different amounts of Ti(O-*t*-Bu)$_4$ were added during synthesis, and it was found that an excess did not increase the thickness of the titania shell but instead resulted in the formation of colloidal titania byproduct. The optimal ratio of titanium(IV) *t*-butoxide to PS beads was determined to be between 4:1 and 8:1 by weight. With a ratio less than 4:1, the titania coverage on the surface of PS beads was found to be nonuniform and produced many broken nanoshells after calcination. At a ratio above 8:1, extensive colloidal TiO$_2$ byproduct contaminated the core−shell nanospheres. This suggested that the growth of the titania shell stopped when the surface of PS beads was covered by a uniform layer of titania. Furthermore, it was observed after calcination that when excess colloidal titania byproduct was present this leads to polydisperse batches according to DLS measurements.

The PS beads within each core−shell nanosphere were removed by calcining at 500 °C for 24 h. The isolated hollow shells (Figure 1C and 1E) were collected and resuspended in ethanol, and a droplet of this solution was used to analyze the NSs with SEM and TEM. The SEM images show no distinguishable shape differences between the formed hollow TiO$_2$ shells doped with and without europium. After calcination there were very few broken undoped hollow TiO$_2$ spheres, and some broken Eu^{3+}-doped spheres can be spotted for doped

shells in their respective image sets (Figure 1C and 1E). The wall thickness of the undoped titania NS was found to be as thin as 5−10 nm, and the results suggest that the doping with Eu^{3+} leads to a more fragile TiO$_2$ shell wall and, therefore, some broken europium-doped NSs. The TEM image (Figure 1F) reveals that small amounts of colloidal TiO$_2$ are fused onto the outer NS surfaces, which was a typical occurrence after the critical shell thickness forms around the aminopolystyrene template.

While preparing the europium-doped titania NS, different concentrations from 0.01% to 0.035% of Eu(NO$_3$)$_3$·5H$_2$O were dissolved in ethanol before adding the aminopolystyrene beads and Ti(O-*t*-Bu)$_4$ to examine how the amount of Eu-(NO$_3$)$_3$·5H$_2$O affects nanoshell synthesis. During the templating reaction, with increasing concentration of Eu(NO$_3$)$_3$·5H$_2$O, the amount of Eu^{3+} trapped in the titania lattice increased, but the NS yield decreased. The percentage doping of Eu^{3+} was confirmed using EDS. Figure 1G shows a typical EDS spectrum of NSs doped with europium(III). Furthermore, when more than 0.035% Eu(NO$_3$)$_3$·5H$_2$O was added during synthesis, it was discovered that templated core−shells were not produced even after 1 h of vortex mixing. The ionic radius of Eu^{3+} (1.087 Å)[57] is significantly greater than that of Ti^{4+} (0.745 Å).[58] It is expected that during polycondensation Eu^{3+} is attracted to the growing anionic TiO$_2$ shell, and at higher concentrations, the significantly larger Eu^{3+} hinders polycondensation and blocks shell growth. Table 1 shows the yield of NS formation and the amount of europium(III) found doped within the different synthesized titania nanosphere batches with the various concentrations of Eu(NO$_3$)$_3$·5H$_2$O added during synthesis. Therefore, to maintain a high NS yield and hollow shell uniformity, it is necessary to limit the amount of Eu-(NO$_3$)$_3$·5H$_2$O added during the sol−gel reaction.

Table 1. Yields of Hollow TiO₂ Nanoshells and Their Europium Content

percentage of Eu(NO₃)₃·5H₂O (%)[a]	0	0.005	0.015	0.025	0.03	0.035
yield % of hollow titania NSs[b]	100	93	82	65	31	~0
theoretical mole percent of Eu(III) in NS[c]	0	0.47	1.40	2.33	2.80	3.26
mole percent of Eu(III) in NSs from EDS	0	0.22	0.34	0.84	1.13	–

[a]Mass percentage of added Eu(NO₃)₃·5H₂O used in the synthesis in ethanol/5% water as wt % of the total solvent. [b]Ratio of hollow europium–titania particles compared with the amount of titania particles obtained by synthesis without added europium (w/w). In this series of experiments, the ratio of titanium(IV) t-butoxide versus PS beads is a constant 6.5:1 (w/w) as the added Eu³⁺ increases. [c]Ratio of added Eu(NO₃)₃·5H₂O compared with added titanium(IV) t-butoxide in the sol–gel reaction.

Electron Microscopy and Dynamic Light Scattering Measurements. Using SEM images (Figure 1), it was found that the average diameter of hollow TiO₂ NSs was slightly smaller than their 200 nm starting PS templates. The size of core–shell and hollow Eu³⁺-doped TiO₂ spheres (doped with 0.025% Eu(NO₃)₃·5H₂O in this set of results) was measured and compared (Table 2). The average diameters of core–shell

Table 2. Average Diameters of Eu³⁺-Doped Core–Shell and Hollow Nanoshells from SEM Images[a]

sample	average diameter (nm)	standard deviation (nm)
Eu³⁺-doped core–shells	200	5
Eu³⁺-doped hollow NSs	185	6

[a]Eu-doped particles were prepared using 0.025% Eu(NO₃)₃·5H₂O during synthesis. Average diameters were calculated by measuring 30 nanospheres in the SEM images.

spheres and hollow spheres were found to be 200 ± 5 and 185 ± 6 nm, respectively (n = 30). After calcination, the TiO₂ shells shrunk by more than 10 nm. This result is consistent with previous measurements of silica nanoshells prepared by a similar template synthesis protocol.[59] This shrinkage likely arises from dehydration of the TiO₂ sol–gel and partial formation of the anatase mineral phase on heating. It is known that dehydration is a common occurrence during the sol–gel drying process.[60] Shrinkage is believed to be isotropic as the shells are uniform in size and shape in the SEM images.

After their dispersal in solution, solution sizes and zeta potentials of core–shell and hollow Eu³⁺-doped TiO₂ spheres

were also determined using dynamic light scattering (DLS). The NSs were suspended at a concentration of 1 mg/mL in distilled water (pH 6.5) and were dispersed using a Misonix ultrasonic liquid processor (XL-2000 series) operating at 5 W with a continuous setting for 60 s at a temperature of 4 °C, before the scattering measurements were taken. The DLS showed average diameters of 305 ± 80 nm (PDI: 0.27) and 310 ± 60 nm (PDI: 0.24) for the doped core–shell and doped hollow NSs, respectively. Their corresponding zeta potentials were 5 and −23 mV. Since the aminopolystyrene beads have a measured zeta potential of −33. mV, these results suggest that Eu³⁺ accumulates on the surface or in the gel coating of the core–shell spheres, with the europium(III) ions eventually being incorporated into the titania lattice on calcination. Core–shell and hollow TiO₂ spheres without Eu³⁺ doping were also measured with DLS. Their respective diameters using intensity-weighted averaging were found to be 250 ± 40 nm (PDI: 0.22) and 240 ± 40 nm (PDI: 0.23), while their zeta potentials were more negative at −44 and −41 mV. The DLS measurements of the aqueous suspensions exhibit slightly increased average hydrodynamic sizes from those determined by SEM measurements, which suggests that the TiO₂ NSs in solution disperse largely as monomers and a small fraction of aggregates; however, the nonideal optical properties of the nanoparticles (a uniform refractive index is assumed in fitting the correlation function) may also distort the measurements. The hollow Eu³⁺-doped TiO₂ NSs were slightly larger than their nondoped TiO₂ NS counterparts. This may be attributed to the lower zeta potential value of the Eu³⁺-doped NS since lower zeta potential values have been shown to correlate with a higher tendency of aggregation.[61]

DLS was used to analyze the PEI-coated Eu/TiO₂ hollow NSs; these particles had an average size of 355 ± 75 nm (PDI: 0.24) with a zeta potential of +46 mV. This indicates that cationic PEI is strongly bound to the negative Eu/TiO₂ NS surface by electrostatic forces, consequently converting the surface charge from negative to positive. In addition, the high positive charge on the PEI-coated NS suggests that the NSs have good stability in aqueous solution,[62] and the low PDI value suggests that the NSs are predominantly monodisperse and that colloidal debris contributes minimally to the sample population.[63] The increase of size from noncoated to PEI-coated NSs can be attributed to the polymer coating (750 000 MW) as the polyoxamer corona surrounding PEI in water has been observed to increase the apparent size when compared to direct measurements (e.g., AFM) of size.[64] A summary of the average diameters of core–shell and hollow NSs measured by DLS analysis can be seen in Table 3.

X-ray Diffraction Measurements. XRD spectra of undoped TiO₂ hollow spheres and various Eu-doped TiO₂

Table 3. Dynamic Light Scattering Measurements of Eu³⁺-Doped and Undoped Core–Shell and Hollow Nanoshells[a]

sample	avg. hydrodynamic diameter (nm)	standard deviation (nm)	PDI (±SD)	zeta potential (mV)
aminopolystyrene (PS) beads	208	4	0.04 ± 0.01	−33
nondoped core–shells	250	40	0.22 ± 0.04	−44
nondoped hollow NS	240	40	0.23 ± 0.07	−41
Eu³⁺-doped core–shells	305	80	0.27 ± 0.05	+5
Eu³⁺-doped hollow NS	310	60	0.24 ± 0.05	−23
PEI-coated Eu³⁺-doped hollow NS	355	75	0.24 ± 0.02	+46

[a]Europium-doped NSs were prepared using 0.025% Eu(NO₃)₃·5H₂O during the synthesis. The average hydrodynamic diameter was based on DLS measurements of three different batches.

hollow NSs are shown in Figure 2. The diffraction pattern matches the International Center for Diffraction Data (ICDD)
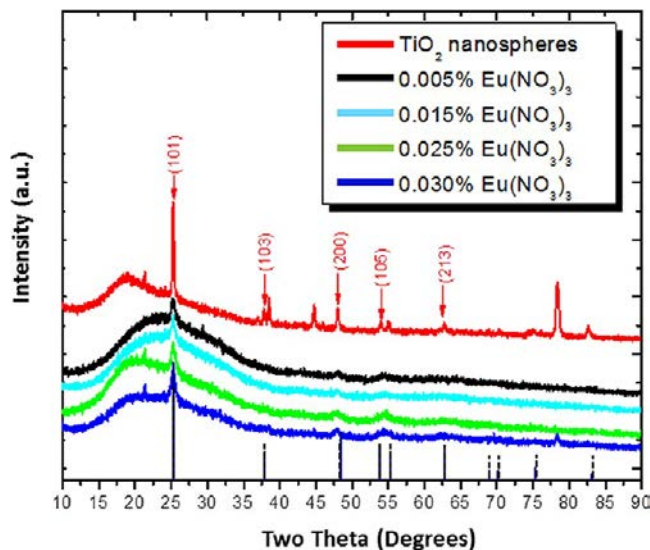
Figure 2. X-ray diffraction patterns of thin films of plain and Eu^{3+}-doped TiO$_2$ hollow nanoshells. The percentages shown are the mass percentage of Eu(NO$_3$)$_3$·5H$_2$O used during the sol−gel synthesis.

sample card 00−001−0562 (shown as vertical lines in Figure 2), which identifies anatase as the predominant titania phase (comparison with ICDD data for the rutile and brookite phases shows that the strongest peak in both is missing) within the NS wall structure. Unmarked peaks have been attributed to the sample holder, and the diffuse background below 35° has been identified as background from the Petrol used to mount the powder. It is observed that the crystalline phase is disturbed by doping with Eu^{3+}, as peak broadening is observed for the anatase phase with only small amounts of Eu^{3+}. This is consistent with structural doping in the lattice by Eu(III) and disruption of the anatase crystal order, rather than merely Eu(III) coating the surface of the titania NS, which would be expected to still show diffraction features of anatase for the underlying TiO$_2$.

Optical Properties. Figure 3 compares the photoluminescence spectra (λ_{ex} = 413 nm) of core−shell and hollow nanoshells made with the same amount of added Eu(NO$_3$)$_3$·5H$_2$O. The $^5D_0$ emission of Eu^{3+} has five characteristic peaks, which are assigned to the $^5D_0−^7F_0$, $^5D_0−^7F_1$, $^5D_0−^7F_2$, $^5D_0−^7F_3$, and $^5D_0−^7F_4$ transitions. The emission of Eu^{3+}-doped TiO$_2$ spheres was dominated by the red emission peak at 617 nm, which is associated with the $^5D_0−^7F_2$ atomic-like f−f transition.[65] There were no other strong emission peaks in the photoluminescence spectra. The emission intensity at 617 nm from calcined hollow NSs was much greater than that of the core−shell spheres having the same content of Eu^{3+}. These results are in agreement with several reports[50,66−68] showing similar emission intensity increases in rare earth doped TiO$_2$ nanoparticles after calcination at ∼500 °C. This was attributed to the structure of TiO$_2$. After calcination at 500 °C, TiO$_2$ is primarily a mixture of anatase and amorphous phases. It has been suggested[44] that the semicrystalline TiO$_2$ structure is an excellent host for Eu^{3+}. The TiO$_2$ nanocrystallite acts as an antenna, and absorbed UV energy is transferred to Eu^{3+}, which sensitizes its luminescence.[44,69] Calcination at temperatures above 500 °C converts TiO$_2$ to the rutile phase, which causes
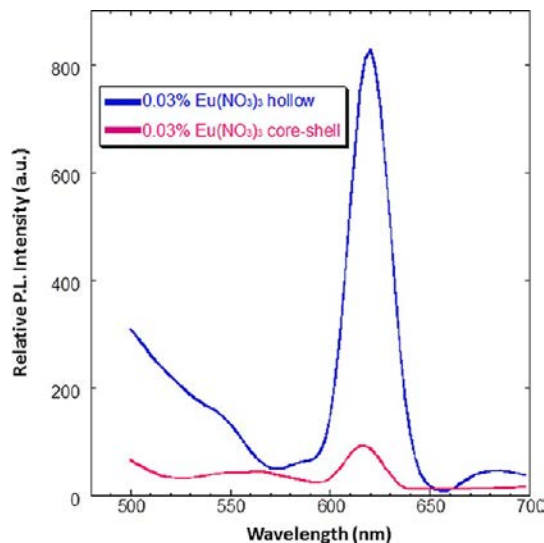
Figure 3. Photoluminescence spectra of Eu^{3+}-doped core−shell and hollow nanoshells. The percentages shown are the mass percentage of Eu(NO$_3$)$_3$·5H$_2$O used during the sol−gel synthesis.

the Eu^{3+} emission to disappear.[69,70] Since europium-doped TiO$_2$ nanoshells emit by a long-lived atomic f−f transition, this offers the possibility of detecting and visualizing their interactions with cells using two-photon (2-P) microscopy, which is an attractive technique for in vitro and in vivo biological imaging since background 2-P bioluminescence is minimal.[71−73]

Endocytosis Experiments. The outer cell surface contains sialic acids, which causes most mammalian cells to have a net anionic surface charge.[74,75] Due to this phenomenon, surface functionalized or coated cationic groups on the surface of microbeads, macromolecules, or nanoparticles cause binding to cells via electrostatic interactions.[76−82] For this reason, Eu−TiO$_2$ NSs were coated with PEI.

The adhesion and uptake of europium-doped TiO$_2$ NSs coated with PEI by HeLa cervical cancer cells under in vitro cell culture conditions was studied and visualized by 2-P microscopy. The cells were marked with green fluorescent CMFDA as the intracellular 2-P stain. Hollow Eu−TiO$_2$ NSs prepared with 0.025% Eu(NO$_3$)$_3$·5H$_2$O during the synthesis reaction (DLS measured average hydrodynamic diameter size of 342 nm and a zeta potential of +46 mV) were employed.

As shown in Figure 4, cells incubated with Eu−TiO$_2$−PEI NSs exhibit a high concentration of red luminescent material surrounding the HeLa cells, while samples incubated with noneuropium-doped TiO$_2$−PEI-functionalized NSs did not and resembled the control HeLa cells. Control samples incubated with noneuropium-doped TiO$_2$−PEI NSs probably have an amount of NSs surrounding the HeLa cells similar to the samples incubated with Eu−TiO$_2$−PEI NSs but are not visible via 2-P microscopy because these control NSs lack red luminescent Eu^{3+}. These imaging results confirm 2-P imaging of the doped nanoparticles and suggest that the red particulates observed around HeLa cells arise due to electrostatic interactions between the positive charged PEI-functionalized Eu−TiO$_2$ NS and the negatively charged glycoproteins found on the cell surface.

To quantify and confirm that these red particle features were due to europium-doped TiO$_2$ NSs and not an optical artifact or bleed over effect from the green dye, the 2-P dual color
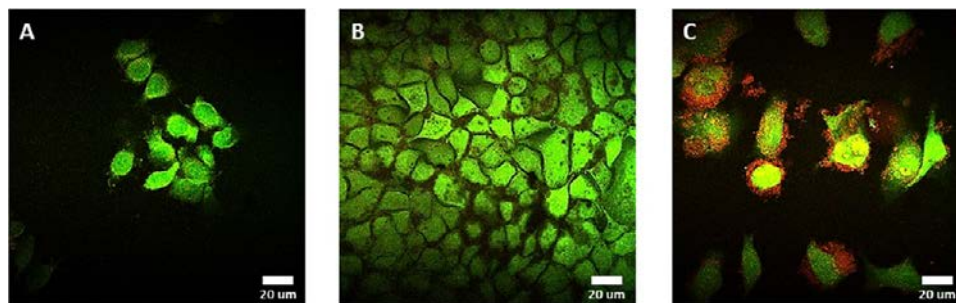
Figure 4. Two-photon microscopy images of nondoped and Eu-doped 200 nm TiO$_2$ nanoshells incubated with HeLa cells. A: HeLa cells, stained with CMFDA (green) dye. B: HeLa cells incubated with 500 μg/mL of undoped TiO$_2$ PEI-coated NSs for 24 h. C: HeLa cells incubated with 500 μg/mL of Eu−TiO$_2$−PEI NSs (red) for 24 h (0.025% Eu(NO$_3$)$_3$·5H$_2$O). Identical settings and gains were used across all microscopy images.
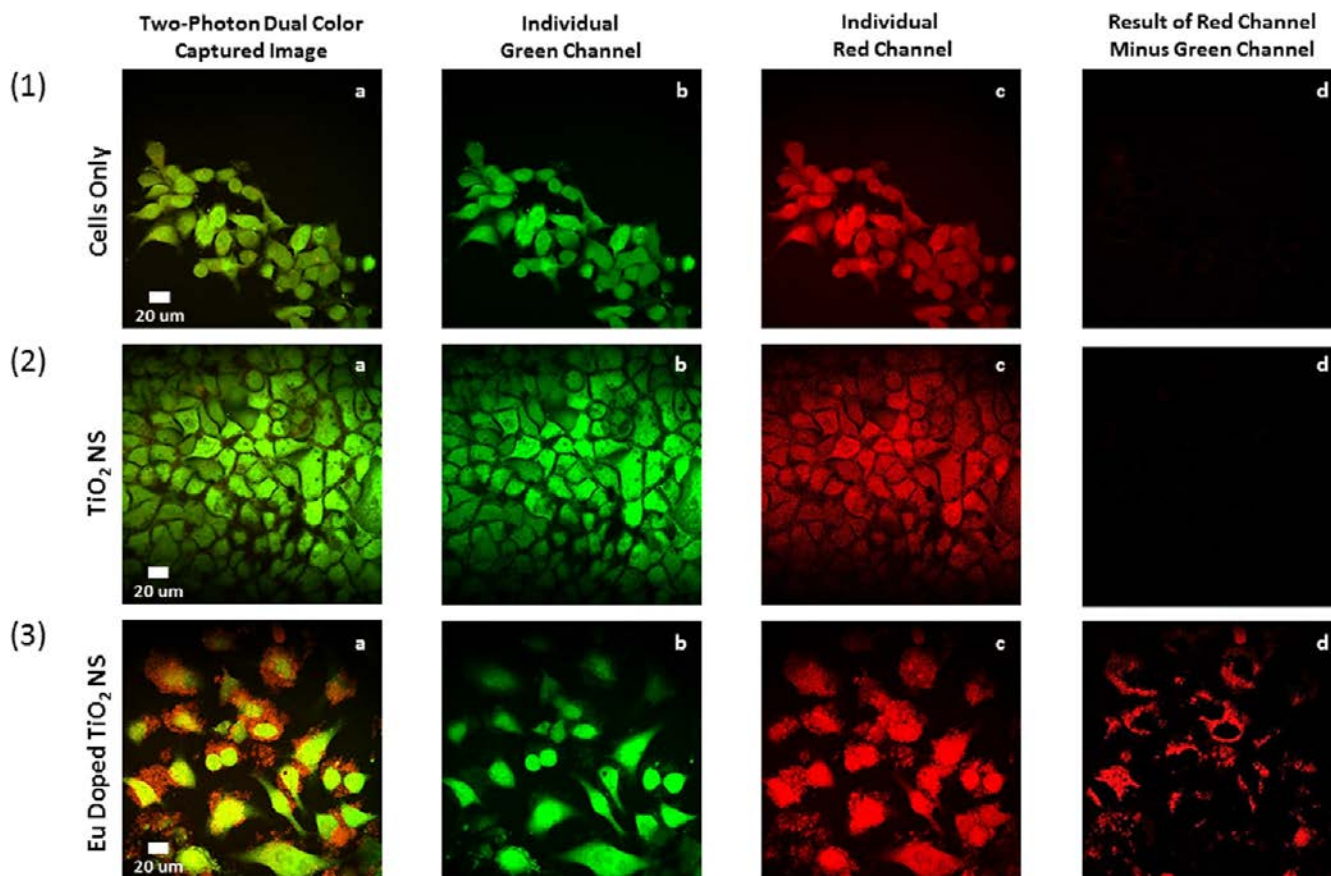
**Figure 5.** Imaging of 200 nm Eu-doped TiO$_2$ nanoshells adhering to HeLa cells. Two-photon dual color captured images of cell only samples (Panel 1a) and cell samples incubated with 500 μg/mL of undoped TiO$_2$−PEI NS (Panel 2a) or Eu−TiO$_2$−PEI NS (Panel 3a). The images were split into their individual green and red image components (1b/1c, 2b/2c, and 3b/3c), and a background subtraction between these images was performed (1d, 2d, 3d) using Image J software.

captured images were split into their individual red, green, and blue channel components, and an image subtraction between each sample's red and green images was performed using Image J software. The intensity values of each pixel in the green fluorescence image were subtracted from each pixel in the red fluorescence image (setting any negative values to zero), leaving only intensity values above and beyond any green fluorescence in the resultant image. As shown Figure 5, the resulting subtracted image for cells incubated with Eu−TiO$_2$−PEI NSs shows a distinct pattern of red luminescence outside of the HeLa cells. Conversely, the cells only and cells incubated with nondoped TiO$_2$−PEI NS samples do not exhibit this red perimeter. Being that all cell samples were prepared and

captured using the same settings, these results establish that this effect is due to cell adhesion of red-emitting PEI-functionalized Eu−TiO$_2$ NSs onto the HeLa cell surface. Furthermore, the red luminescence pattern exhibits variations in thickness, which suggests there are one or multiple NS layers on the cell surface. This is consistent with previous results showing a similar thick multilayered nanoparticle surface adhesion pattern under confocal microscopy[83,84] or SEM analysis[85] when nanoparticle endocytosis is not favored. Whether endocytosis occurs can depend on the cell type,[14,86−89] nanoparticle size,[90−95] nanoparticle shape,[83,92,96−98] and/or presence of ligands on the nanoparticle surface that facilitate cell surface receptor mediated pathways.[99−103]
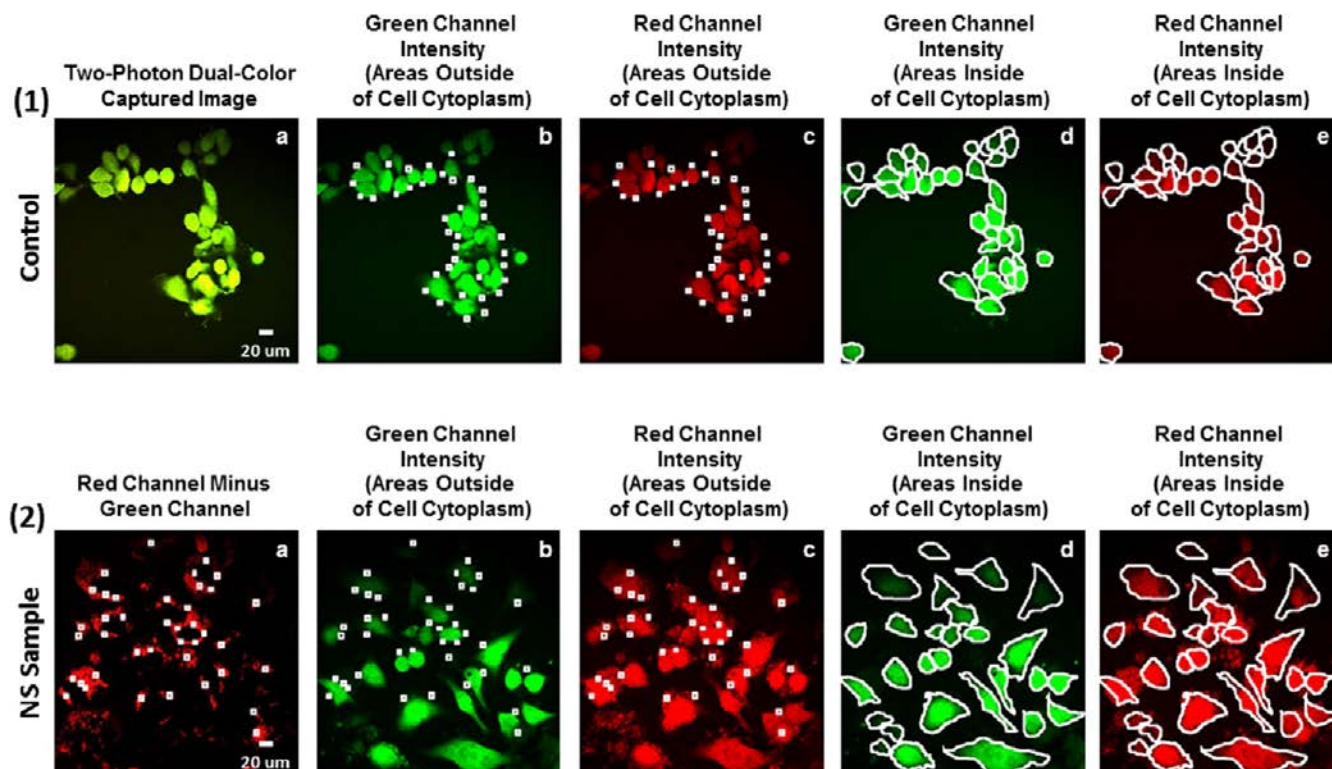
Figure 6. Luminescence intensity ratio analysis of nanoshell cell adhesion/endocytosis from Figure 5. Panel 1: Green and red channel images of outlines of areas just outside (1b and 1c) or inside (1d and 1e) HeLa cells for a control sample. Panel 2: Corresponding image outlines for cells incubated with 200 nm Eu–TiO$_2$–PEI NSs. All outlines were based on the location of the green cytoplasmic cell stain images and then used to calculate the fluorescence ratios in Table 4.

A luminescence ratio analysis was performed on the outer and inner regions of the cell membrane to distinguish between the amount of PEI NS attached to the outer part of the membrane and those internalized by cells. This use of the red to green luminescence ratio to establish NS adhesion/endocytosis has been described.[55] Briefly, the luminescence ratio analysis was performed using Image J to first create cytoplasmic cell outlines to determine the extent of NS internalization by cells or locationization in small rectangular regions just outside the green CMFDA stain cells to demonstrate NS cell adhesion (Figure 6). The cell outlines were based on the individual green channel images and were applied to the same location/coordinates on their red channel counterparts by using the ROI manager in Image J. The Image J analyze/measure tools were used to determine the mean luminescence values inside the cell outlines or in rectangular regions just outside the cells for both the green and red channels, which in turn were used to calculate the red to green luminescence ratio either inside or just outside the cells.

The ratio analysis performed on the regions just outside of HeLa-only samples showed a red/green luminescence ratio value of 1.42 (SE ± 0.03), while the HeLa cell samples incubated with europium-doped TiO$_2$ NSs exhibited a ratio of 4.29 (±0.15) (Table 4). Thus, the cells incubated with Eu–TiO$_2$ NSs had a photoluminescence intensity ratio ~200% greater in areas just outside the cellular membrane than control HeLa cells. This suggests that a large number of Eu^{3+}-doped hollow titania NSs attached to the outer surface of HeLa cells through electrostatic interactions. Moreover, when the ratio analysis was performed on the interior areas of cells, the HeLa-only samples had a ratio of 1.07 (±0.02), whereas samples that

Table 4. Luminescence Intensity Ratio Analysis for 200 nm PEI-Coated TiO$_2$ NSs Made Using 0.025% Eu(NO$_3$)$_3$·5H$_2$O^a

	red mean luminescence/green mean luminescence	standard error
controls: outside of cell^b (n = 118)	1.42	0.03
NS samples: outside of cell (n = 93)	4.29	0.15
controls: inside of cell^c (n = 122)	1.07	0.02
NS samples: inside of cell (n = 48)	1.56	0.11

^{a}Note: Luminescence ratios inside and outside of cells for control samples are different because inner cell ratios were calculated in areas where the cell is stained (ratio most likely bleeds through into red of green dye), while outer cell ratios were calculated in nonstained (i.e., black background) areas. ^{b}Outside of Cell = red/green luminescence ratios calculated using small outline boxes surrounding a cell like those seen in Figure 6 (panels 1b,2b and 1d,2d). ^{c}Inside of Cell = red/green luminescence ratios calculated using cytoplasmic cell outline like those seen in Figure 6 (panels 1c,2c and 1e,2e).

saw Eu–TiO$_2$ NSs had a value of 1.56 (±0.11). Therefore, cells that were incubated with NSs were 46% more luminescent, which is consistent with a small amount of Eu–TiO$_2$ NSs being endocytosed by HeLa cells. These ratio analysis values are similar to those obtained for adhesion/endocytosis of Eu^{3+}-doped hollow silica NSs.[55] Emission from Eu^{3+}-doped hollow titania NSs is more intense than for the corresponding silica NSs.

CONCLUSION

Uniform-sized Eu^{3+}-doped hollow titania NSs were fabricated by a new method using $Ti(O-t-Bu)_4$ and $Eu(NO_3)_3$ with amine-functionalized polystyrene beads serving as templates. Removal of the polystyrene core by calcining led to increased luminescence from Eu^{3+}-doped hollow nanoshells as the hydrated titania sol–gel partially transformed to the anatase-doped crystalline phase. Up to 1.1% Eu^{3+} could be introduced before the nanoshells lost their structural integrity, and the doped NS exhibited a strong narrow red photoluminescence emission at 617 nm upon UV excitation of the titania. Europium-doped hollow NSs were functionalized with PEI, which changed the NS surface charge from negative to positive. The positively charged doped NSs were shown by two-photon microscopy to bind to the outer surface of HeLa cervical cancer cells with minimal endocytosis. Since the Eu^{3+} luminescence does not photobleach, the UV absorbing titania acts as an antenna to enhance emission, and the luminescent state is also amenable to imaging by two-photon techniques. These NSs may be especially useful in the fields of biological imaging, diagnostics, and/or therapeutics.

AUTHOR INFORMATION

Corresponding Author
*E-mail: wtrogler@ucsd.edu.

Notes
The authors declare no competing financial interest.

ACKNOWLEDGMENTS

REFERENCES

(1) Ma, L.; Liu, M.; Peng, T.; Fan, K.; Lu, L.; Dai, K. *Mater. Chem. Phys.* **2009**, *118*, 477.
(2) Vlachopoulos, N.; Liska, P.; Augustynski, J.; Graetzel, M. *J. Am. Chem. Soc.* **1988**, *110*, 1216.
(3) Mohammadi, M. R.; Fray, D. J.; Cordero-Cabrera, M. C. *Sens Actuators, B* **2007**, *124*, 74.
(4) Xu, J.; Ao, Y.; Fu, D.; Yuan, C. *Colloids Surf. A* **2009**, *334*, 107.
(5) Li, Y.; Kunitake, T.; Fujikawa, S. *J. Phys. Chem. B* **2006**, *110*, 13000.
(6) Lee, S.-A.; Choo, K.-H.; Lee, C.-H.; Lee, H.-I.; Hyeon, T.; Choi, W.; Kwon, H.-H. *Ind. Eng. Chem. Res.* **2001**, *40*, 1712.
(7) Park, Y.; Lee, S.-H.; Kang, S. O.; Choi, W. *Chem. Commun.* **2010**, *46*, 2477.
(8) Arabatzis, I. M.; Falaras, P. *Nano Lett.* **2002**, *3*, 249.
(9) Macak, J. M.; Tsuchiya, H.; Ghicov, A.; Yasuda, K.; Hahn, R.; Bauer, S.; Schmuki, P. *Curr. Opin. Solid State Mater. Sci.* **2007**, *11*, 3.
(10) Cao, J.; Rusina, O.; Sieber, H. *Ceram. Int.* **2004**, *30*, 1971.
(11) Necula, B. S.; Fratila-Apachitei, L. E.; Zaat, S. A. J.; Apachitei, I.; Duszczyk, J. *Acta Biomater.* **2009**, *5*, 3573.
(12) Tsuang, Y.-H.; Sun, J.-S.; Huang, Y.-C.; Lu, C.-H.; Chang, W. H.-S.; Wang, C.-C. *Artif. Organs* **2008**, *32*, 167.
(13) Paunesku, T.; Rajh, T.; Wiederrecht, G.; Maser, J.; Vogt, S.; Stojicevic, N.; Protic, M.; Lai, B.; Oryhon, J.; Thurnauer, M.; Woloschak, G. *Nat. Mater.* **2003**, *2*, 343.
(14) Thurn, K.; Brown, E.; Wu, A.; Vogt, S.; Lai, B.; Maser, J.; Paunesku, T.; Woloschak, G. *Nanoscale Res. Lett.* **2007**, *2*, 430.
(15) Roy, S. C.; Paulose, M.; Grimes, C. A. *Biomaterials* **2007**, *28*, 4667.
(16) Zhu, R. R.; Wang, S. L.; Chao, J.; Shi, D. L.; Zhang, R.; Sun, X. Y.; Yao, S. D. *Mater. Sci. Eng., C* **2009**, *29*, 691.
(17) Lopez, T.; Figueras, F.; Manjarrez, J.; Bustos, J.; Alvarez, M.; Silvestre-Albero, J.; Rodriguez-Reinoso, F.; Martinez-Ferre, A.; Martinez, E. *Eur. J. Med. Chem.* **2010**, *45*, 1982.
(18) Kubota, Y.; Shuin, T.; Kawasaki, C.; Hosaka, M.; Kitamura, H.; Cai, R.; Sakai, H.; Hashimoto, K.; Fujishima, A. *Br. J. Cancer* **1994**, *70*, 1107.
(19) Kalbacova, M.; Macak, J. M.; Schmidt-Stein, F.; Mierke, C. T.; Schmuki, P. *Phys Status Solidi-R* **2008**, *2*, 194.
(20) Trouiller, B.; Reliene, R.; Westbrook, A.; Solaimani, P.; Schiestl, R. H. *Cancer Res.* **2009**, *69*, 8784.
(21) Chen, W.; Zhang, J. *J. Nanosci. Nanotechnol.* **2006**, *6*, 1159.
(22) Rozhkova, E. A.; Ulasov, I.; Lai, B.; Dimitrijevic, N. M.; Lesniak, M. S.; Rajh, T. *Nano Lett.* **2009**, *9*, 3337.
(23) Abdulla-Al-Mamun, M.; Kusumoto, Y.; Islam, M. S.; Yang, H. *Chem. Lett.* **2009**, *38*, 950.
(24) Abdulla-Al-Mamun, M.; Kusumoto, Y.; Islam, M. S. *Chem. Lett.* **2009**, *38*, 980.
(25) Abdulla-Al-Mamun, M.; Kusumoto, Y. *Chem. Lett.* **2009**, *38*, 826.
(26) Lopez, T.; Recillas, S.; Guevara, P.; Sotelo, J.; Alvarez, M.; Odriozola, J. A. *Acta Biomater.* **2008**, *4*, 2037.
(27) Xu, J.; Sun, Y.; Huang, J.; Chen, C.; Liu, G.; Jiang, Y.; Zhao, Y.; Jiang, Z. *Bioelectrochemistry* **2007**, *71*, 217.
(28) Caruso, R. A.; Susha, A.; Caruso, F. *Chem. Mater.* **2001**, *13*, 400.
(29) Meyer, U.; Larsson, A.; Hentze, H. P.; Caruso, R. A. *Adv. Mater.* **2002**, *14*, 1768.
(30) Zhong, Z.; Yin, Y.; Gates, B.; Xia, Y. *Adv. Mater.* **2000**, *12*, 206.
(31) Lei, Z.; Li, J.; Ke, Y.; Zhang, Y.; Zhang, H.; Li, F.; Xing, J. *J. Mater. Chem.* **2001**, *11*, 2930.
(32) Kim, T. H.; Lee, K. H.; Kwon, Y. K. *J. Colloid Interface Sci.* **2006**, *304*, 370.
(33) Sun, X.; Liu, J.; Li, Y. *Chem.—Eur. J.* **2006**, *12*, 2039.
(34) Wang, D.; Song, C.; Lin, Y.; Hu, Z. *Mater. Lett.* **2006**, *60*, 77.
(35) Yang, Z.; Niu, Z.; Lu, Y.; Hu, Z.; Han, C. C. *Angew. Chem., Int. Ed.* **2003**, *42*, 1943.
(36) Blešić, M. D.; Šaponjić, Z. V.; Nedeljković, J. M.; Uskoković, D. P. *Mater. Lett.* **2002**, *54*, 298.
(37) Karan, N. S.; Agrawal, A.; Pandey, P. K.; Smitha, P.; Sharma, S. J.; Mishra, D. P.; Gajbhiye, N. S. *Mater. Sci. Eng., B* **2009**, *163*, 128.
(38) Zhang, C.; Zhang, J.; Zhang, X.; Feng, X.; Chen, J.; Han, B.; Yang, G. *J. Supercrit. Fluid* **2007**, *42*, 142.
(39) Wu, C.-I.; Huang, J.-W.; Wen, Y.-L.; Wen, S.-B.; Shen, Y.-H.; Yeh, M.-Y. *Mater. Lett.* **2008**, *62*, 1923.
(40) Bouzigues, C.; Gacoin, T.; Alexandrou, A. *ACS Nano* **2011**, *5*, 8488.
(41) Lo, W. S.; Kwok, W. M.; Law, G. L.; Yeung, C. T.; Chan, C. T. L.; Yeung, H. L.; Kong, H. K.; Chen, C. H.; Murphy, M. B.; Wong, K. L.; Wong, W. T. *Inorg. Chem.* **2011**, *50*, 5309.
(42) Conde-Gallardo, A.; Garcia-Rocha, M.; Hernandez-Calderon, I.; Palomino-Merino, R. *Appl. Phys. Lett.* **2001**, *78*, 3436.
(43) Li, J.-G.; Wang, X.; Watanabe, K.; Ishigaki, T. *J. Phys. Chem. B* **2006**, *110*, 1121.
(44) Yin, J. B.; Xiang, L. Q.; Zhao, X. P. *Appl. Phys. Lett.* **2007**, *90*.
(45) Ghosh, P.; Patra, A. *J. Phys. Chem. C* **2007**, *111*, 7004.

(46) Julian, B.; Corberan, R.; Cordoncillo, E.; Escribano, P.; Viana, B.; Sanchez, C. *Nanotechnology* **2005**, *16*, 2707.

(47) Luo, M.; Cheng, K.; Weng, W.; Song, C.; Du, P.; Shen, G.; Xu, G.; Han, G. *Nanoscale Res. Lett.* **2009**, *4*, 809.

(48) Aihua, P.; Erqing, X.; Changwen, J.; Ran, J.; Hongfeng, L. *Mater. Lett.* **2005**, *59*, 3866.

(49) Tan, M.; Wang, G.; Ye, Z.; Yuan, J. *J. Lumin.* **2006**, *117*, 20.

(50) Xu, Z.; Yang, Q.; Xie, C.; Yan, W.; Du, Y.; Gao, Z.; Zhang, J. *J. Mater. Sci.* **2005**, *40*, 1539.

(51) Yi, S.-s.; Bae, J. S.; Moon, B. K.; Jeong, J. H.; Kim, J. H. *Opt. Mater.* **2006**, *28*, 610.

(52) Zhao, Z.; Zeng, Q. G.; Zhang, Z. M.; Ding, Z. J. *J. Lumin.* **2006**, *122−123*, 862.

(53) Andelman, T.; Gordonov, S.; Busto, G.; Moghe, P. V.; Riman, R. E. *Nano Res. Lett.* **2010**, *5*, 263.

(54) Epling, G. A.; Lin, C. *Chemosphere* **2002**, *46*, 561.

(55) Yang, J.; Sandoval, S.; Alfaro, J. G.; Aschemeyer, S.; Liberman, A.; Martin, D. T.; Makale, M.; Kummel, A. C.; Trogler, W. C. *J. Biomed. Opt.* **2011**, *16*, 066012-1.

(56) Gash, A. E.; Tillotson, T. M.; Satcher, J. H., Jr.; Hrubesh, L. W.; Simpson, R. L. *J. Non-Cryst. Solids* **2001**, *285*, 22.

(57) Klimchuk, O.; Atamas, L.; Miroshnichenko, S.; Kalchenko, V.; Smirnov, I.; Babain, V.; Varnek, A.; Wipff, G. *J. Inclusion Phenom. Macrocyclic Chem.* **2004**, *49*, 47.

(58) Tong, T.; Zhang, J.; Tian, B.; Chen, F.; He, D. *J. Hazard Mater.* **2008**, *155*, 572.

(59) Yang, J.; Lind, J. U.; Trogler, W. C. *Chem. Mater.* **2008**, *20*, 2875.

(60) Brinker, C. J.; Scherer, G. W. *Sol-gel science: the physics and chemistry of sol-gel processing*; Academic Press: Boston, 1990.

(61) Suvarna, S.; Espinasse, B.; Qi, R.; Lubica, R.; Poncz, M.; Cines, D. B.; Wiesner, M. R.; Arepally, G. M. *Blood* **2007**, *110*, 4253.

(62) *Zeta Potential of Colloids in Water and Waste Water*; American Society for Testing and Materials (ASTM) Standard D 4187-8, 1985.

(63) Bazylińska, U.; Warszyński, P.; Wilk, K. A. *Colloids Surf. A: Physicochem. Eng. Aspects* **2012**, DOI: 10.1016/j.colsurfa.2011.12.006.

(64) Thuenemann, A. F.; Mueller, M.; Dautzenberg, H.; Joanny, J.-F.; Loewen, H. *Adv. Polym. Sci.* **2004**, *166*, 113.

(65) Werts, M. H. V. *Sci. Prog.* **2005**, *88*, 101.

(66) Jeon, S.; Braun, P. V. *Chem. Mater.* **2003**, *15*, 1256.

(67) Feng, X.; Yang, L.; Zhang, N.; Liu, Y. *J. Alloys Compd.* **2010**, *506*, 728.

(68) Ding, S.; Huang, F.; Mou, X.; Wu, J.; Lu, X. *J. Mater. Chem.* **2011**, *21*, 4888.

(69) Pal, M.; Pal, U.; Jimenez, J. M. G. Y.; Perez-Rodriguez, F. *Nanoscale Res Lett* **2012**, *7*, 1.

(70) Ningthoujam, R. S.; Sudarsan, V.; Vatsa, R. K.; Kadam, R. M.; Jagannath; Gupta, A. *J. Alloys Compd.* **2009**, *486*, 864.

(71) Kim, H. M.; Fang, X. Z.; Yang, P. R.; Yi, J.-S.; Ko, Y.-G.; Piao, M. J.; Chung, Y. D.; Park, Y. W.; Jeon, S.-J.; Cho, B. R. *Tetrahedron Lett.* **2007**, *48*, 2791.

(72) Sumalekshmy, S.; Fahrni, C. J. *Chem. Mater.* **2010**, *23*, 483.

(73) Eliseeva, S. V.; Bunzli, J.-C. G. *Chem. Soc. Rev.* **2010**, *39*, 189.

(74) Yacobi, N. R.; Malmstadt, N.; Fazlollahi, F.; DeMaio, L.; Marchelletta, R.; Hamm-Alvarez, S. F.; Borok, Z.; Kim, K. J.; Crandall, E. D. *Am. J. Respir. Cell Mol.* **2010**, *42*, 604.

(75) Finkelstein, E. I.; Chao, P.-h. G.; Hung, C. T.; Bulinski, J. C. *Cell Motil. Cytoskeleton* **2007**, *64*, 833.

(76) Cohen, C. M.; Kalish, D. I.; Jacobson, B. S.; Branton, D. *J. Cell Biol.* **1977**, *75*, 119.

(77) Kalish, D. I.; Cohen, C. M.; Jacobson, B. S.; Branton, D. *Biochim. Biophys. Acta* **1978**, *506*, 97.

(78) Schroeder, A.; Levins, C. G.; Cortez, C.; Langer, R.; Anderson, D. G. *J. Intern. Med.* **2010**, *267*, 9.

(79) Daniels, D. S.; Schepartz, A. *J. Am. Chem. Soc.* **2007**, *129*, 14578.

(80) Frankel, A. D.; Pabo, C. O. *Cell* **1988**, *55*, 1189.

(81) Hong, S.; Bielinska, A. U.; Mecke, A.; Keszler, B.; Beals, J. L.; Shi, X.; Balogh, L.; Orr, B. G.; Baker, J. R., Jr.; Banaszak Holl, M. M. *Bioconjugate Chem.* **2004**, *15*, 774.

(82) Karmali, P. P.; Chaudhuri, A. *Med. Res. Rev.* **2007**, *27*, 696.

(83) Huang, X.; Teng, X.; Chen, D.; Tang, F.; He, J. *Biomaterials* **2010**, *31*, 438.

(84) Huang, M.; Ma, Z.; Khor, E.; Lim, L.-Y. *Pharm. Res.* **2002**, *19*, 1488.

(85) Gupta, A. K.; Curtis, A. S. G. *Biomaterials* **2004**, *25*, 3029.

(86) Cai, Y.; Liu, Y.; Yan, W.; Hu, Q.; Tao, J.; Zhang, M.; Shi, Z.; Tang, R. *J. Mater. Chem.* **2007**, *17*, 3780.

(87) Mansouri, S.; Cuie, Y.; Winnik, F.; Shi, Q.; Lavigne, P.; Benderdour, M.; Beaumont, E.; Fernandes, J. C. *Biomaterials* **2006**, *27*, 2060.

(88) de Salamanca, A. E.; Diebold, Y.; Calonge, M.; García-Vazquez, C.; Callejo, S.; Vila, A.; Alonso, M. J. *Invest. Ophthalmol. Visual Sci.* **2006**, *47*, 1416.

(89) Cartiera, M. S.; Johnson, K. M.; Rajendran, V.; Caplan, M. J.; Saltzman, W. M. *Biomaterials* **2009**, *30*, 2790.

(90) Slowing, I. I.; Vivero-Escoto, J. L.; Wu, C. W.; Lin, V. S. Y. *Adv. Drug Delivery Rev.* **2008**, *60*, 1278.

(91) Desai, M. P.; Labhasetwar, V.; Walter, E.; Levy, R. J.; Amidon, G. L. *Pharm. Res.* **1997**, *14*, 1568.

(92) Chithrani, B. D.; Ghazani, A. A.; Chan, W. C. W. *Nano Lett.* **2006**, *6*, 662.

(93) Prabha, S.; Zhou, W. Z.; Panyam, J.; Labhasetwar, V. *Int. J. Pharm.* **2002**, *244*, 105.

(94) Zhang, S.; Li, J.; Lykotrafitis, G.; Bao, G.; Suresh, S. *Adv. Mater.* **2009**, *21*, 419.

(95) Jiang, W.; Betty, Y. S. K.; Rutka, J. T.; Chan, W. C. W. *Nat. Nano* **2008**, *3*, 145.

(96) Verma, A.; Stellacci, F. *Small* **2010**, *6*, 12.

(97) Muro, S.; Garnacho, C.; Champion, J. A.; Leferovich, J.; Gajewski, C.; Schuchman, E. H.; Mitragotri, S.; Muzykantov, V. R. *Mol. Ther.* **2008**, *16*, 1450.

(98) Perry, J. L.; Herlihy, K. P.; Napier, M. E.; DeSimone, J. M. *Acc. Chem. Res.* **2011**, *44*, 990.

(99) Tkachenko, A. G.; Xie, H.; Coleman, D.; Glomm, W.; Ryan, J.; Anderson, M. F.; Franzen, S.; Feldheim, D. L. *J. Am. Chem. Soc.* **2003**, *125*, 4700.

(100) Byrne, J. D.; Betancourt, T.; Brannon-Peppas, L. *Adv. Drug Delivery Rev.* **2008**, *60*, 1615.

(101) Davis, M. E. *Mol. Pharm.* **2009**, *6*, 659.

(102) Berry, C. C. *J. Mater. Chem.* **2005**, *15*, 543.

(103) Rosenholm, J. M.; Meinander, A.; Peuhu, E.; Niemi, R.; Eriksson, J. E.; Sahlgren, C.; Lindén, M. *ACS Nano* **2008**, *3*, 197.